ISSN 1392–1320 MATERIALS SCIENCE (MEDŽIAGOTYRA). Vol. 30, No. 2. 2024

Near-infrared Spectrum Characteristics of Micro-Nano Material Based Diffraction Optical Devices

Zhao JIN [1], Qiyao XIAO [2], Yue ZHANG [2], Cheng SUN [2, 3], Yongbo DENG [4], Chengmiao WANG [4], Qiang FU [1], Yingchao LI [1], Huilin JIANG [1] *

[1] *School of Opto-electric Engineering, Changchun University of Science and Technology, Changchun 130022, China;*
[2] *College of Physical Science and Technology, Dalian University, Dalian 116622, China*
[3] *Liaoning Engineering Laboratory of Optoelectronic Information Technology, Dalian 116023, China*
[4] *State Key Laboratory of Applied Optics (SKLAO), Changchun Institute of Optics, Fine Mechanics and Physics (CIOMP), Chinese Academy of Sciences, Changchun 130033, China*

http://doi.org/10.5755/j02.ms.35151

Received 21 September 2023; accepted 14 November 2023

Diffractive optics devices are optical devices in which the amplitude or phase of the incident light is spatially modulated periodically by a micro-nanomaterial based structure. The study of diffractive optics devices in the field of micro and nano can change the spectroscopic behavior of micro and nano diffractive optics devices by varying the microstructure of the structure and the optical wave properties, which can effectively and reasonably modulate the optical wave signal. To study the effect of different parameter structures on the performance of micro-nano diffraction optical devices, in this paper, two three-dimensional array structures of diffractive optical devices are proposed, which are a vertex-intersecting regular tetrahedron structure and a base-intersecting regular frustum structure. Using the Finite-Difference Time-Domain method, the spectroscopic images of the diffractive optics of the constructed micro-nano diffractive devices are studied in the near-infrared band by varying the height of the constructed structures, the type of structures, the wavelength of the incident light waves, and the polarization direction of the light waves in different 3D height coordinates. The effects of different parameter changes on the performance of the micro-nano diffractive optics devices were analyzed by image comparison. The results show that the best diffraction effect is achieved at a structure height of 0.9 μm for both models with different structure types. The study of both structures at this structure height reveals that the location of diffraction occurrence and the intensity of diffraction can be tuned by varying the structure and the relevant parameters such as the polarization of the light wave. This paper has some theoretical applications for the study of high-performance diffractive optics.
Keywords: near-infrared, finite-difference time-domain, diffractive optics micro and nanostructures, diffractive properties.

1. INTRODUCTION

Diffractive Optical Elements (DOEs), also known as binary optical elements, modulate the phase of light propagation through the design of different surface microstructures. Due to their unique surface micro-nano structure design, DOEs can achieve functionalities that traditional optical systems cannot, offering advantages such as high efficiency, high precision, low weight, and small size [1 – 3]. In practical applications of laser shaping, DOEs are widely used and play an influential role in laser homogenization, collimation, focusing, and pattern formation [4].

DOEs have lightweight and planar geometries, providing significant advantages over traditional refractive optical elements. With the progress of micro-nano fabrication technology [5], DOEs can now be manufactured on a large scale with at low cost. Therefore, DOEs have found widespread applications in various fields such as imaging, optical communications, and lithography. In current research, the manufacturing of DOEs has been achieved through light-assisted trapping and patterned nanoparticles [6 – 7]. Recent studies have demonstrated that this approach can produce diffractive gratings with periods as short as a few micrometers. Due to the maturity of the current technology, the micro-nano structural design and performance analysis of DOEs in this paper hold certain theoretical value for fabricating well-established DOEs.

In the preliminary research of our team, it was found that diffraction gratings can alter the optical properties, such as transmittance, of incident light. This makes them suitable for the design of various optical devices, including surfaces of thin-film solar cells [8, 10, 18, 19]. Building upon this foundation, this paper primarily focuses on systematically studying the electromagnetic field distribution at wavelengths where a specific diffraction grating exhibits significant changes in transmittance under incident light. The goal is to identify regions with enhanced electromagnetic fields in different structures, providing a theoretical basis for further development and design of related optical devices. The specific research will revolve around the design of surface micro/nano structures for diffractive optical devices. By varying parameters such as height, structure type, wavelength of incident light, and polarization direction, spectroscopic images of the constructed micro/nano diffractive optical devices will be studied at different three-dimensional height coordinates. Through comparative analysis of these images, the impact

* Corresponding author. Tel.: +86-13604405267. fax: +86-411-87402712.
E-mail address: *hljiang@cust.edu.cn* (H. Jiang)

of parameter variations on the performance of micro/nano diffractive optical devices will be assessed.

2. STRUCTURE AND METHOD

This paper presents two diffractive optical micro-nano structure models. One is a vertex-intersecting regular tetrahedron structure, and the remaining is a base-intersecting regular frustum structure. Both structures are made of SiO_2 and arranged in regular arrays. In the subsequent numerical simulations, the constructed models are treated as a unit and an array model is created by connecting infinite units for numerical simulation. The grating period was 1.0 μm, and the used refraction index was 1.46 for SiO_2.

The Finite-Difference Time-Domain (FDTD) method [9, 12] is applied in this study for simulation. This method is based on the fundamental Maxwell equations in electrodynamics and directly calculates the numerical solution based on the temporal electromagnetic field differential equations. It has been widely used in electromagnetics, electronics, and optics [11].

Since the focus of this research is on the diffractive optical performance of the structures, plane waves that allow simultaneous analysis of the electric and magnetic fields in the same plane are employed for simulation and analysis. The light source is incident from below the substrate, along the positive z-axis direction, as shown in Fig. 1. The wavelength of the plane wave is set between 800 nm and 1500 nm, covering the near-infrared range. To ensure accurate numerical simulation, grid parameter optimization is performed. Through preliminary experiments, a grid accuracy of 10 nm was validated and deemed suitable for the study. Ultimately, a grid accuracy of 10 nm is set for all three axes (x, y, z); periodic boundary conditions are applied in the x and y directions, while perfect matching layer (PML) boundary conditions are applied in the z direction.

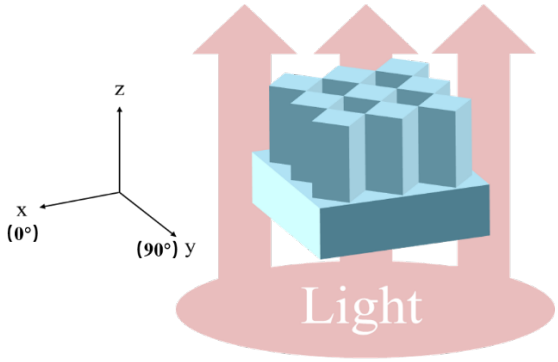

Fig. 1. Simulation model

3. ANALYSIS OF SIMULATION RESULTS

3.1. Varying structure height

First, we conducted a study on the diffraction optical performance of the regular tetrahedral prism structure and made adjustments to the constructed basic model. We investigated the differences in the diffraction performance of the model under different heights of the tetrahedral prism. Fig. 2 shows the schematic diagram of the regular tetrahedral prism models with different heights. The constructed regular tetrahedral prisms only differed in height. We set up 11 regular tetrahedral prisms with different heights, increasing the height incrementally. The height h of the models in the Fig. 2 increases sequentially, with an increment of 0.1 μm. A total of 11 tetrahedral prism models were set up, ranging from a height of 0.5 μm to 1.5 μm, to explore the influence of different heights of regular tetrahedral prism arrays on diffraction performance. We conducted 11 sets of experiments with regular tetrahedral prisms of different heights and obtained a graph showing the relationship between the transmittance of light and wavelength, as shown in Fig. 3. Furthermore, we determined the optimal wavelength and the appropriate height of the regular tetrahedral prism for achieving the best diffraction effect.

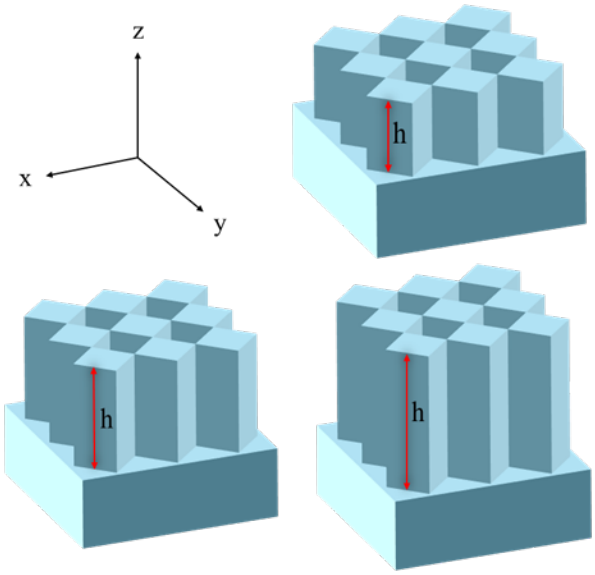

Fig. 2. The height h of the normal quadrilateral model increases successively with an increasing interval of 0.1 μm. A total of 11 quadrilateral models are set, and the height increases successively from 0.5 μm to 1.5 μm

The base material and regular tetrahedral prism material in the simulation are both SiO_2. After measurement, the transmittance of SiO_2 in the near-infrared wavelength range of 800 nm to 1500 nm is found to be 0.97. If the transmittance of the light wave significantly decreases after constructing the structure in the experiment, it indicates that a diffraction effect is occurring. By varying the height of the regular tetrahedral prism while keeping the diagonal length of each prism base at 1.0 μm, the height h of the prism increases sequentially from 0.5 μm to 1.5 μm. The transmittance of light waves with different wavelengths passing through prisms of different heights is measured, and the relationship between wavelength and transmittance is obtained.

Considering 1.0 μm as the threshold, the data is divided into two groups to further analyze the influence of height on diffraction performance. The first group includes the results within the range of 0.5 μm to 1.0 μm, as shown in Fig. 3. In summary, from Fig. 3, it can be observed that within the wavelength range of 800 nm – 1000 nm, the diffraction effects of different heights on the structure are not significant. However, for different structure heights, a sharp

decrease in transmittance occurs between the wavelengths of 950 nm and 1000 nm, reaching the lowest transmittance at 1002 nm.

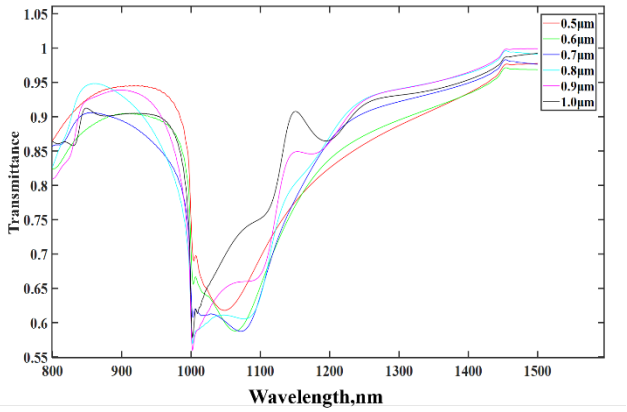

Fig. 3. Relationship between transmittance and wavelength of 0.5 μm – 1.0 μm height regular quadrilateral prism

Within the wavelength range of 1000 nm – 1200 nm, the transmittance curves for structure heights of 0.5 μm, 0.6 μm, 0.7 μm, and 0.8 μm are similar, with two distinct transmittance dips. The peak of the second dip is higher than the first dip, indicating a weakening of diffraction effects at the wavelength of the second dip. For structure heights of 0.9 μm and 1.0 μm, no second transmittance dip is observed between 1000 nm and 1200 nm, suggesting that the diffraction effects of the structure vary with height. When the wavelength exceeds 1200 nm, the transmittance curves for different structure heights are similar, with only slight differences in transmittance levels, indicating a diminishing impact of different structure heights on diffraction performance with increasing wavelength.

Fig. 4 shows the transmittance spectra for different heights ranging from 1.0 μm to 1.5 μm. From Fig. 4, it can be observed that within the wavelength range of 800 nm – 1000 nm, the transmittance curves for structure heights of 1.1 μm – 1.5 μm are similar.

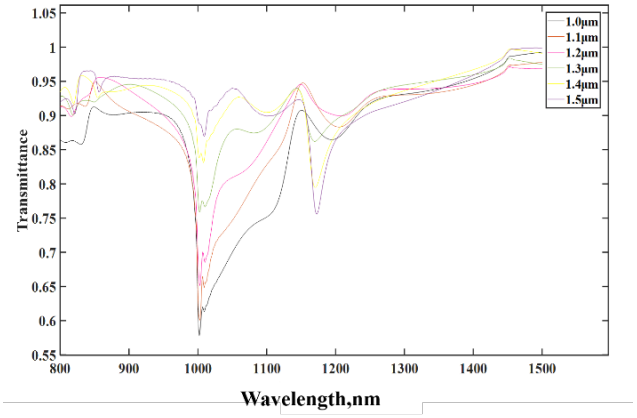

Fig. 4. Relationship between transmittance and wavelength of 1.0 μm – 1.5 μm height regular quadrilateral prism

The transmittance for a structure height of 1.0 μm has a lower dip around 800 nm, but the transmittance is still relatively high, indicating that the diffraction effects of the device are still not significant at this height. For different structure heights, a sharp decrease in transmittance occurs between the wavelengths of 950 nm and 1000 nm, reaching the lowest transmittance at 1002 nm. Within the wavelength range of 1000 nm – 1150 nm, the transmittance-wavelength relationship curves for structure heights of 1.0 μm – 1.5 um are similar. Within this range, as the structure height gradually increases, the transmittance also increases for the same wavelength, indicating a gradual weakening of diffraction effects with increasing structure height in this wavelength range. Within the wavelength range of 1150 nm – 1200 nm, all different heights exhibit a minor dip, with a structure height of 1.5 μm showing the lowest transmittance. When the wavelength exceeds 1250 nm, the transmittance curves for different structure heights are similar, with only slight differences in transmittance levels, indicating a diminishing impact of different structure heights on diffraction performance with increasing wavelength.

3.2. Varying the structure shape

The second part of the simulation will involve varying the structure of the model. Based on the optimal wavelength obtained in the first part for diffraction effects in a regular tetrahedral array, the wavelength of the light wave will be kept constant while the model's structure is modified. A regular tetrahedral prism with connected bases will be constructed to study the effect of varying the model's structure on diffraction performance. Fig. 5 a shows a 3D view of the regular tetrahedral prism, with $h_1 = 0.9$ μm. Fig. 5 b depicts a top view of the regular tetrahedral prism, with $D_1 = 1$ μm, where the vertices of the tetrahedron intersect.

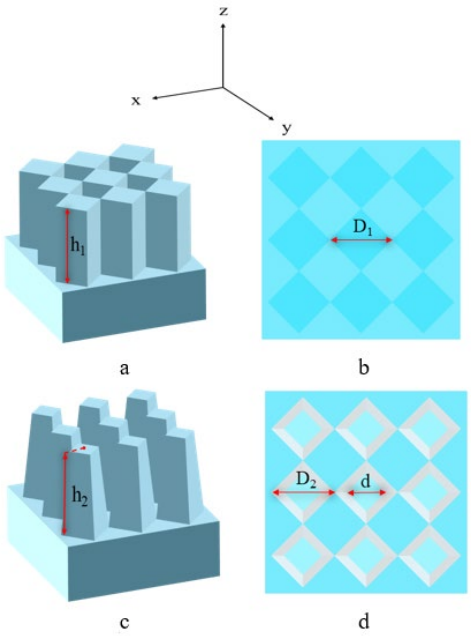

Fig. 5. Comparison of a regular quadrilateral column and a regular quadrilateral platform of the same height

Fig 5 c illustrates a 3D view of the regular tetrahedral frustum, with the same height as the regular tetrahedral prism, $h_2 = 0.9$ μm. Fig. 5 d displays a top view of the regular tetrahedral frustum, with $D_2 = 1$ μm, where the bottom vertices of the frustum are connected and the top of the frustum has a distance of d = 0.707 μm.

Further study the difference of different models at 1002 nm wavelength and 0.9μm height to explore the impact on the performance of diffracted optical elements, as shown in Fig. 6.

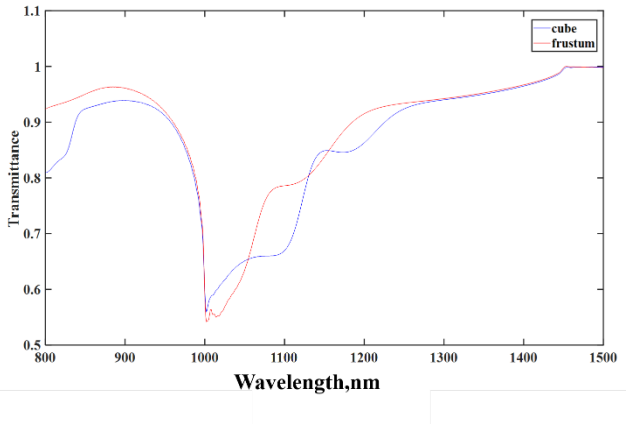

Fig. 6. Relation between transmittance and wavelength of 0.9 μm height regular quadrilateral prism and regular quadrilateral platform

According to Fig. 6, it can be seen that both the transmission rates of the regular tetrahedron with a height of 0.9 μm and the regular frustum with a height of 0.9 μm reach the lowest point at a wavelength of 1002 nm. This indicates that both structures achieve optimal diffraction at a height of 0.9 μm and a wavelength of 1002 nm. Therefore, an experiment should be conducted to compare the diffraction performance of the two structures at a wavelength of 1002 nm and a height of 0.9 μm.

3.3. Varying the polarization direction of light

Firstly, the differences in electric field distribution between a regular tetrahedron and a regular tetrahedron frustum at different diffraction positions were studied when the polarization direction of light was set to 0°. Electric field monitors were placed at the bottom of the models, specifically at a height coordinate of z = 0 μm, and at the top of the models, specifically at a height coordinate of z = 0.9 μm. The experimental results are shown in Fig. 7.

Fig. 7 a shows the electric field distribution of a right square prism at a height coordinate z = 0 μm, with the polarization direction of the light at 0°; Fig. 7 b shows the electric field distribution of a right square prism at a height coordinate z = 0.9 μm, with the polarization direction of the light at 0°; Fig. 7 c shows the electric field distribution of a right square pyramid at a height coordinate z = 0 μm, with the polarization direction of the light at 0°; Fig. 7 d shows the electric field distribution of a right square pyramid at a height coordinate z = 0.9 μm, with the polarization direction of the light at 0°.

From Fig. 7 a and c, it can be seen that at a wavelength of 1002 nm, for a prism with a height of 0.9 μm and a height coordinate of z = 0 μm, the position of the strongest electric field is mainly along the y-axis when the polarization direction of the light is 0°, at the upper and lower vertices of the bottom surface of the prism. Comparing Fig. 7 a with Fig. 7 b, it can be found that for the same structure under the same wavelength and polarization, the distribution of the position of the strongest electric field at different height coordinates is different, as shown in Fig. 7 b and d. When the height coordinate is z = 0.9 μm, the position of the strongest electric field is mainly along the x-axis, at the left and right vertices of the top surface of the prism. Moreover, with different height coordinates, the maximum values of the electric field strength are also different. The maximum field strength at z = 0.9 μm is stronger than the maximum field strength at z = 0 μm.

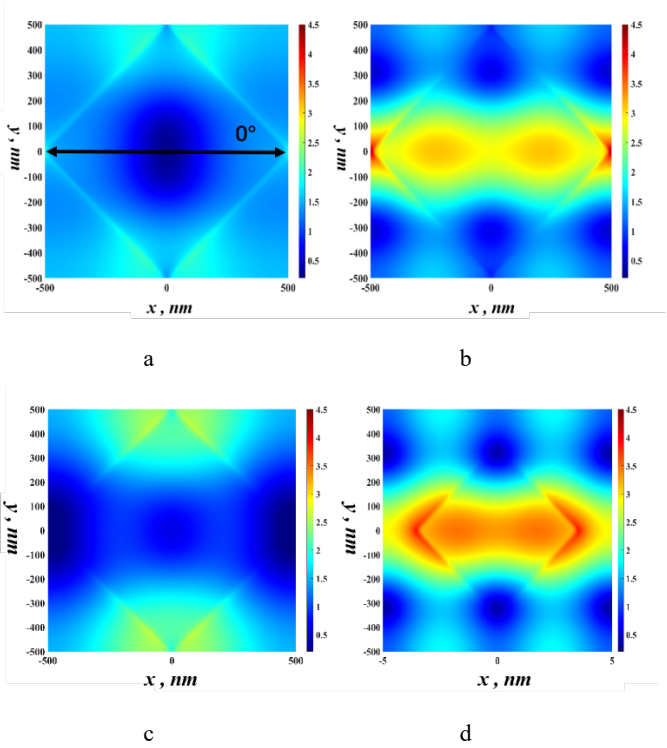

Fig. 7. Electric field distribution of 0°polarized light incident structure

Under the condition that other parameters remain unchanged, varying the shape of the structure results in similar diffraction patterns. For both the prism array and the pyramid array, at a height coordinate of z = 0 μm and a polarization direction of 0°, diffraction occurs mainly along the y-axis, at the upper and lower vertices of the bottom surface of the prism. At a height coordinate of z = 0.9 μm, the diffraction positions of both structures rotate by 90° and occur mainly along the x-axis, at the left and right vertices of the top surface of the prism. However, the changes in the structures will affect the magnitude and uniformity of the diffracted electric field. There is a significant difference in uniformity between the two structures, with only weak diffraction occurring at the center of the prism structure, but continuous and more uniform diffraction occurring at the center of the pyramid, with an increase in the intensity of the central diffraction.

Furthermore, varying the polarization of the light to a direction of 45°, while keeping the structural parameters and the position of the electric field monitor consistent with the 0° polarization direction, allows for observing the differences in the electric field performance of the diffraction elements with different structures at the same height.

Fig. 8 a shows the electric field distribution of a right square prism at a height coordinate of z = 0 μm, with the

polarization direction of light at 45°; Fig. 8 b shows the electric field distribution of a right square prism at a height coordinate of z = 0.9 μm, with the polarization direction of light at 45°; Fig. 8 c shows the electric field distribution of a right square pyramid at a height coordinate of z = 0 μm, with the polarization direction of light at 45°; Fig. 8 d shows the electric field distribution of a right square pyramid at a height coordinate of z = 0.9 μm, with the polarization direction of light at 45°.

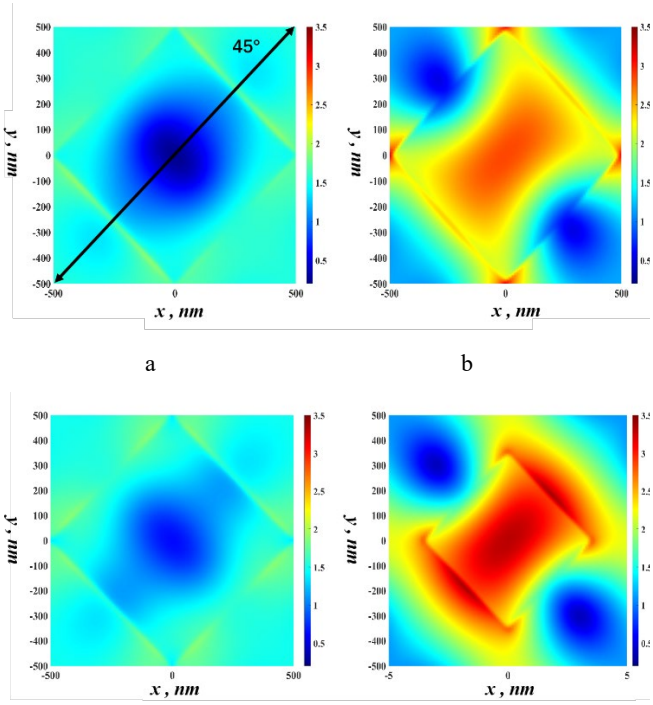

Fig. 8. Electric field distribution of 45°polarized light incident structure

From Fig. 8, it can be observed that at a wavelength of 1002 nm, with a height of 0.9 μm and a height coordinate of z = 0 μm, the strongest electric field intensity is mainly located at the four vertices of the bottom surface of the regular tetrahedron. Additionally, there is also a strong electric field distribution around the vertices, while the central part has almost no electric field distribution. Comparing Fig. 8 a with b and Fig. 8 c with d, it can be found that at z = 0.9 μm, there is still a strong electric field distribution in the central part of the structure. The maximum field intensity varies with different height coordinates, with the maximum field intensity at z = 0.9 μm being stronger than the maximum field intensity at z = 0 μm. Unlike the diffraction occurring mainly at the four vertices on both the top and bottom surfaces of the tetrahedron, on the bottom surface of the structure, diffraction mainly occurs at the four vertices, while on the top surface of the structure, diffraction occurs on the two sides of the square.

Finally, the polarization of the light wave was changed to 90°, and the structural parameters of the two models and the placement of the electric field monitor remained consistent with the 0° polarization direction. The differences in the electric field performance of the diffraction elements with different structures at the same structural height were observed, as shown in Fig. 9.

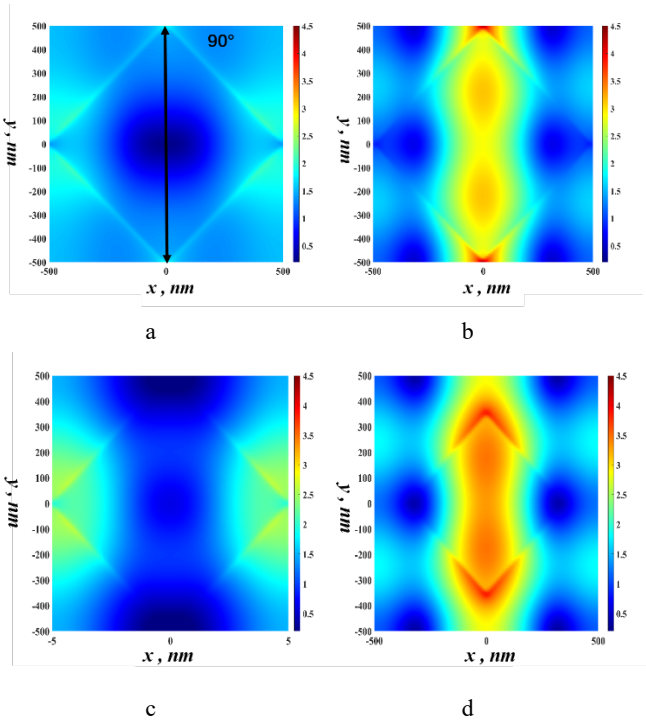

Fig. 9. Electric field distribution of 90°polarized light incident structure

Fig. 9 a shows the electric field distribution of a right square prism at a height coordinate z = 0 μm, with the polarization of light at 90°. Fig. 9 b shows the electric field distribution of a right square prism at a height coordinate z = 0.9 μm, with the polarization of light at 90°. Fig. 9 c shows the electric field distribution of a right square pyramid at a height coordinate z = 0 μm, with the polarization of light at 90°. Fig. 9 d shows the electric field distribution of a right square pyramid at a height coordinate z = 0.9 μm, with the polarization of light at 90°.

From Fig. 9 a, it can be seen that at a wavelength of 1002 nm, with a height of 0.9 μm, at a height coordinate of z = 0 μm, and with a polarization direction of 90°, the position of the strongest electric field intensity is mainly along the x-axis, at the left and right vertices of the bottom surface of the regular prism. By observing Fig. 9 b, it can be found that at a height position of z = 0.9 μm, the position of the strongest electric field intensity is mainly along the y-axis, at the top and bottom vertices of the top surface of the regular prism. By comparing Fig. 9 a with Fig. 9 b, it can be found that for the same structure, under the same wavelength and polarization, the distribution of the position of the strongest electric field intensity varies with different height coordinates. Moreover, with different height coordinates, the maximum value of the electric field intensity is also different, and the maximum field strength at z = 0.9 μm is significantly stronger than that at z = 0 μm. Similar results can also be observed from Fig. 9 c and d, compared to Fig. 9 a and b.

Once again, by comparing Fig. 9, it can be concluded that under the same conditions, varying the shape of the structure leads to similar diffraction patterns. For both regular prism arrays and regular pyramid arrays, at a height coordinate of z=0μm and with a polarization direction of 0°,

diffraction occurs mainly along the x-axis, at the left and right vertices of the bottom surface of the regular prism. At a height coordinate of z = 0.9 μm, the diffraction positions of both structures rotate by 90° and occur mainly along the y-axis, at the top and bottom vertices of the top surface of the regular prism. However, the changes in the two structures will affect the magnitude and uniformity of the diffracted electric field. From the Fig. 9, it can be clearly seen that at a height coordinate of z = 0 μm, the maximum value of the electric field for the regular pyramid structure is greater than that for the regular prism structure. Moreover, the diffraction uniformity at the top and bottom vertices of the regular pyramid structure is better than that of the regular prism structure. The regular prism structure only exhibits weak diffraction at the center, while the regular pyramid structure shows continuous and more uniform diffraction at the center, with an increase in the intensity of the central diffraction.

By comparing Fig. 7 a, c, Fig. 8 a, c, Fig. 9 a, and c, it can be observed that the diffraction positions of different structures with the same wavelength, structure height, height coordinate, and polarization direction are roughly the same. Fig. 7 a and c show the electric field distribution at a height coordinate of z = 0 μm under 0° polarization direction. It can be seen that the diffraction mainly occurs along the y-axis, at the upper and lower vertices of the intersection of the regular prism. Fig. 9 a and c show the electric field distribution at a height coordinate of z = 0 μm under 90° polarization direction. It can be seen that the diffraction mainly occurs along the x-axis, at the left and right vertices of the intersection of the regular prism. Compared to the diffraction positions under 0° polarization direction in Fig. 7 a and c, the diffraction positions under 90° polarization direction in Fig. 9 a and c have rotated by 90°. The significant difference between 0° and 90° polarization directions is the 45° polarization direction. Fig. 8 a and c show the electric field distribution at a height coordinate of z = 0 μm under 45° polarization direction. Under 45° polarization, the diffraction occurs at the four vertices of the prism. Compared to 0° and 90° polarization directions, the overall diffraction is more uniform, and the maximum intensity of the electric field is lower.

Fig. 7 b, d, Fig. 8 b, d, Fig. 9 b and d show the electric field distribution at a height coordinate of z = 0.9 μm. Fig. 7 b and d only change the height coordinate compared to Fig. 7 a and c, and the diffraction positions have rotated by 90°. It changes from mainly occurring along the y-axis at the upper and lower vertices of the intersection of the regular prism to mainly occurring along the x-axis at the left and right vertices of the intersection of the regular prism. Similarly, Fig. 9 b and d only change the height coordinate compared to Fig. 9 a and c, and the diffraction positions have rotated by 90°. It changes from mainly occurring along the x-axis at the left and right vertices of the intersection of the regular prism to mainly occurring along the y-axis at the upper and lower vertices of the intersection of the regular prism. Therefore, it can be seen that there are two methods to change the diffraction positions in the 0° and 90° polarization directions: varying the polarization direction of light or varying the height coordinate. Under the 45° polarization direction, the diffraction occurs at the four vertices, so there is not much difference between the polarization positions at the top and bottom of the structure. However, the diffraction phenomenon is more concentrated and the electric field intensity is higher at the top, while the diffraction phenomenon is more uniform and the electric field intensity is lower at the bottom.

4. CONCLUSIONS

This article presents the micro-nano structures of two diffraction optical elements, one is a SiO_2 regular tetrahedral array structure, and the other is a SiO_2 regular tetrahedron array structure. By using the numerical simulation method of finite difference time domain, the transmittance and electric field distribution of the two structures are studied in the near-infrared wavelength range by varying the height, shape, electric field monitoring position of the structure, as well as the wavelength and polarization direction of the incident light. The diffraction performance parameters of the two structures are obtained. The results show that there is a significant difference in the diffraction performance of the structures with the same structure but different heights. Moreover, at the same structure height, there are also significant differences in diffraction performance at different height coordinates. The study on controlling variables for the two different structures shows that by adjusting the structure, the diffraction of the structure can exhibit either uniform distribution or concentrated distribution.

At present, in this field, researchers have carried out extensive research on the optical properties of micro-nano grating structures. This includes studies on filter polarizers based on grating structures [13, 14], investigations into the diffraction behavior of surface plasmon waves on metasurfaces [15], simulation studies on the reflection characteristics of microstructures with different unit sizes, research on generating cylindrical vector-polarized light using subwavelength nanostructured grating devices [16], and the optical characterization of anti-reflective grating structures using the FDTD method [17], among others. However, there are no reports yet on simulating the transmission efficiency and electric field distribution in the infrared region for a series of micro/nano structured metasurfaces based on regular tetrahedral prism structures, as presented in this paper.

However, by using the research results of this paper, optical uniformizers or devices that concentrate optical energy can be fabricated to improve the performance of lasers. The structures constructed in this experiment have different transmittance parameters at different heights, and the diffraction optical elements with the desired transmittance can be designed by utilizing the structural parameters. The theoretical results of this article have reference value for the design of high-performance diffraction optical elements using SiO_2 materials.

Acknowledgments

This work has been supported by the National Natural Science Foundation of China (No. 61890960).

REFERENCES

1. **Stern, L., Bopp, D.G., Schima, S.A., Maurice, V.N., Kitching, J.E.** Chip-scale Atomic Diffractive Optical Elements *Nature Communications* 10 (1) 2019: pp. 3156 – 3157. https://doi.org/10.1038/s41467-019-11145-5
2. **Yu, N., Capasso, F.** Flat Optics with Designer metasurfaces *Nature Materials* 13 (2) 2014: pp. 139 – 50. https://doi.org/10.1038/nmat3839
3. **Liu, W.J., Hui, P., Cao, A., Shi, L., Deng, Q.** Design and Experiments of Annular Bean Shaping Device with Low Speckle Noise *Acta Photonica Sinica* 49 (02) 2020: pp. 99 – 107. https://doi.org/10.3788/gzxb20204902.0222001
4. **Kazanskiy, N.L., Khonina, S.N., Karpeev, S.V., Porfirev, A.P.** Diffractive Optical Elements for Multiplexing Structured Laser Beams *Quantum Electronics* 50 (7) 2020: pp. 629 – 635. https://doi.org/10.1070/QEL17276
5. **Muñoz-Martínez, J.F., Jubera, M., Matarrubia, J., García-Cabañes, A., Agulló-López, F., Carrascosa, M.** Diffractive Optical Devices Produced by Light-assisted Trapping of Nanoparticles *Optics Letters* 41 (2) 2016: pp. 432 – 435. https://doi.org/10.1364/OL.41.000432
6. **Burgos, H., Jubera, M., Villarroel, J., García-Cabañes, A., Agulló-López, F., Carrascosa, M.** Role of Particle anisotropy and Deposition Method on the Patterning of Nano-objects by the Photovoltaic Effect in $LiNbO_3$ *Optical Materials* 35 (9) 2013: pp. 1700 – 1705. https://doi.org/10.1016/j.optmat.2013.04.035
7. **Villarroel, J., Burgos, H., García-Cabañes, Á., Carrascosa, M., Blázquez-Castro, A., Agulló-López, F.** Photovoltaic Versus Optical Tweezers *Optics Express* 19 (24) 2011: pp. 24320 – 24330. https://doi.org/10.1109/10.1364/oe.19.024320
8. **Sun, C., Wang, Z., Wang, X., Liu, J.** A Surface Design for Enhancement of Light Trapping Efficiencies in Thin Film Silicon Solar Cells *Plasmonics* 11 2016: pp. 1003 – 1010. https://doi.org/10.1007/s11468-015-0135-8
9. **Allen, T., Susan, C., Hagness, X.** Computational Electrodynamics *Artech House Inc* 2000: pp. 200 – 232.
10. **Zhang, K.** The Simulation of Localized Surface Plasmon Modes of Metal Nanoparticles. Hefei; University of Science and Technology of China, 2018.
11. **Fan, W., Chen, Z.Z., Yang, S.C.** On the Analytical Solution of the FDTD Method *IEEE Transactions on Microwave Theory and Techniques* 64 (11) 2016: pp. 3370 – 3379. https://doi.org/10.1109/TMTT.2016.2604310
12. **Mai, H., Chen, J., Xu, X., Zhang, A.** A Novel Hybrid Algorithm Based on FDTD and WCS-FDTD Methods *International Journal of RF and Microwave Computer - Aided Engineering* 30 (5) 2020: pp. 1-16. https://doi.org/10.1002/mmce.22166
13. **Xu, T., Wu, Y.K., Luo, X.** Plasmonic Nanoresonators for High-resolution Colour Filtering and Spectral Imaging *Nature Communications* 1 2010: pp. 59 – 63. https://doi.org/10.1038/ncomms1058
14. **Ellenbogen, Y., Seo, K., Crozier, K.B.** Chromatic Plasmonic Polarizers for Active Visible Color Filtering and Polarimetry *Nano Letters* 12 (2) 2012: pp. 1026 – 1031. https://doi.org/10.1021/nl204257g.
15. **Wang, X.F., Lu, Z.W., Wang, T.S., Yu, W.X.** Grating Diffractive Behavior of Surface Plasmon Wave on Meta-surface *Chinese Optics* 11 (1) 2018: pp. 60 – 73. https://doi.org/10.3788/CO.20181101.0060
16. **Zhon, G.Z.,** Study on Generation of Cylindrical Vector Beam by Using Subwavelength Nanostructured Grating Polarizer, XiAn: Northwestem Polytechnical University, 2019.
17. **Hao, P.** Research on Analysis and Experiment of Some Micro-Nano Devices' Optical Properties, HeFei; PhD thesis. University of Science and Technology of China, 2012
18. **Zhang, T., He, J., Xie, W., Sun, C.** Plasmonic Properties of a Honeycomb Structure Formed by Metallic Nanoparticles *Physica E Low-dimensional Systems and Nanostructures* 118 2019: pp. 113901. https://doi.org/10.1016/j.physe.2019.113901
19. **Zhang, Q., Zhang, Y., Xiong, T., Wang, W., Sun, C.** Plasmonic Properties of Gold Central Symmetrical Tetramer in the Visible Regime *Plasmonics (Norwell, Mass.)* 18 (5) 2018: pp.1959 – 1969. https://doi.org/10.1007/s11468-023-01911-z